Journal of
Materials Chemistry C

PAPER

View Article Online
View Journal | View Issue

Cite this: J. Mater. Chem. C, 2015, 3, 5795

Toward a new generation of white phosphors for solid state lighting using glassy yttrium aluminoborates†

Vinicius Ferraz Guimarães,[ab] Lauro J. Q. Maia,[c] Isabelle Gautier-Luneau,[ab] Christophe Bouchard,[ab] Antonio Carlos Hernandes,[d] Fabrice Thomas,[e] Alban Ferrier,[fg] Bruno Viana[f] and Alain Ibanez*[ab]

Received 23rd January 2015,
Accepted 7th May 2015

DOI: 10.1039/c5tc00237k

www.rsc.org/MaterialsC

We present a new family of highly emissive white phosphors. These phosphors are based on original glassy yttrium aluminoborates (g-YAB) compositions, obtained at low temperatures without any melting, from non-toxic and low cost precursors through the generic polymeric precursor method. Their photoluminescence (PL) arises from structural defects, whose energy levels are widely extended within the large bandgap of these materials. One of the main objectives of this work, is to enhance the point defect concentrations by accurately controlling the powder annealing (temperature and atmosphere) in order to generate intense and broadband PL. Moreover, these g-YAB powders exhibit excellent thermal and chemical stabilities and tunable PL properties, from bluish to warm white emissions, by simply adjusting the annealing temperatures. We determined the internal quantum yields of g-YAB powders using near ultraviolet excitations, which reached values above 90%. We quantified the relative amounts of point defects by electronic paramagnetic resonance and their distribution within the bandgap by means of thermally stimulated luminescence and we directly correlated this defect density to the PL properties. Finally, based on these promising lighting properties, a prototype was firstly developed to estimate the lighting performances of this new g-YAB phosphors family.

1 Introduction

Through the development of GaN and InGaN-based light emitting diodes (LEDs) in the near ultraviolet (NUV) and blue wavelengths, solid-state lighting (SSL) is considered a major disruptive technology for general illumination.[1,2] This is due to several promising properties of white light emitting diodes (WLEDs) such as particularly high luminous efficiency, energy saving, long lifetimes and applicability.[3,4] Nevertheless, one of the main remaining challenges is the discovery of more efficient orange-red emitting phosphors, for the down conversion of nearly monochromatic emissions of NUV or blue LEDs, to produce comfortable and safe warm white lightings. An alternative to rare earth or transition metals activators based phosphors[5] is to use a full-color emitting, single-phase such as phosphors involving structural defects acting as emitting centers (color centers). Thus, since pioneering works,[6] silica-based materials have been the focus of important research efforts.[6–9] It has been shown that this silica phosphors can produce broadband emissions (bluish-white) in the visible range with internal quantum yields (iQY) ranging from 20 to 45% under NUV excitation (365 nm). The source of the photoluminescence (PL) properties was ascribed to carbon-related defects.[6] After silica, several other metal oxides have been studied (zirconates,[10] aluminates,[11–13] alumino-silicates,[14] tungstates,[15,16] tin and zinc oxides[17,18]) as well as, phosphate materials, such as BPO_4 (purple or blue emissions under NUV excitations[19]) and boronitride or borooxynitride compounds (BN or BNO phosphors). In these later cases, it has been shown that upon doping, carbon substitutes boron or nitrogen in the BCNO framework thus increasing the point defect concentration correlated with the PL efficiency.[20,21]

Although the PL mechanisms are not yet fully understood in those defect-related materials, it seems that these emissions

[a] Univ. Grenoble Alpes, Inst NEEL, F-38042 Grenoble, France. E-mail: alain.ibanez@neel.cnrs.fr
[b] CNRS, Inst NEEL, F-38042 Grenoble, France
[c] Instituto de Física, Universidade Federal de Goiás/UFG, C.P. 131, 74001-970, Goiânia/GO, Brazil
[d] Instituto de Física de São Carlos, Universidade de São Paulo/USP, C.P. 369, 13560-970, São Carlos/SP, Brazil
[e] Département de Chimie Moléculaire, Chimie Inorganique Redox (CIRE), UMR CNRS 5250, Université Grenoble Alpes, B.P. 53, 38041 Grenoble Cedex 9, France
[f] PSL Research University, Chimie ParisTech, CNRS, Institut de Recherche de Chimie Paris, 75005, Paris, France
[g] UPMC Univ Paris 06, F-75005, Paris, France

† Electronic supplementary information (ESI) available. See DOI: 10.1039/c5tc00237k

result from specific defects such as vacancies (particularly oxygen vacancies), impurities (mainly carbon atoms) or radicals (peroxyl, $CO_2^{\bullet -}$), which create energy levels within the bandgap of the material.[22] Even if these previous results have shown that this new type of phosphors is promising for the development of SSL devices, these materials exhibit blue or bluish-white PL emissions corresponding to cold and uncomfortable lightings, and their quantum efficiencies were generally not accurately specified.

Based on these first studies of defect-related PL materials, we have recently undertaken the development of new aluminoborate phosphors. Our first objective was to promote the creation of a wide variety of defects and their local surroundings in the glass network, leading to the formation of extended energy levels within the bandgap and to related PL broadband. The second purpose of this study, directly coupled to the first one, was to manage the number of structural defects and so strongly amplify the PL. We started from glassy yttrium aluminoborate compositions close to the stoichiometry of the c-YAB crystal ($YAl_3(BO_3)_4$), which exhibits a wide bandgap of around 6.2 eV. Aluminoborate systems favor extended glass-forming regions in the corresponding phase diagrams to widely adjust the chemical composition to tune the PL properties. The aluminoborate glassy frameworks also present a high variety of short and intermediate range orders. Aluminum can be in AlO_4, AlO_5 or AlO_6 sites,[23–25] while boron can form a large variety of chains or rings based on BO_3 or BO_4 basic units.[23–25] This results in a huge diversity of possible point defects (different type of vacancy or substitution each with different possible atomic surroundings) and should favor broad PL emission in the whole visible region to produce warm-white emissions.[26] Finally, aluminoborates matrices are stable, non-toxic, constituted by abundant elements and can be produced inexpensively on a large scale by several approaches, such as sol–gel or polymeric precursor methods also called modified Pechini process.[27]

2 Experimental section

2.1 Sample preparation and characterizations

For the preparation of glassy aluminoborate powders we selected the polymeric precursor (PP) method. $Y(NO_3)_3{\cdot}6H_2O$ (2.68 g, 7 mmol, 99.9%, Strem Chemicals), $Al(NO_3)_3{\cdot}9H_2O$, (7.88 g, 21 mmol, 99.8%, Fischer Scientific) and citric acid (32.28 g, 168 mmol, 99.5%, Sigma-Aldrich) were dissolved in deionized water (50 mL, at 80 °C during 30 min under stirring). In a second solution, H_3BO_3 (1.73 g, 28 mmol, 99.8%, Fischer Scientific) and d-sorbitol (20.40 g, 112 mmol, 99.5%, Sigma) were dissolved in deionized water (50 mL). The molar ratio citric acid: Y : Al : B: d-sorbitol was kept to 24 : 1 : 3 : 4 : 16. These two solutions were then mixed together and placed under reflux at 105 °C during 24 hours to assure the complete polymerization reactions of reagents. Then, the solution was evaporated at 90 °C to reach about 40% of the initial volume, leading to a yellowish and viscous resin ready to be dried and annealed. These resins were gradually dried at 250 °C, during 30 min, under air atmosphere, in a tubular furnace. The resulting puffs were crushed to obtain fine brown powders, which were then pyrolysed under N_2 atmosphere at 700 °C during 24 hours. This intermediate partial oxidation led to amorphous black powders that were then calcinated at different temperatures (T_{ca}) between 650 and 780 °C for 24 hours under O_2 atmosphere, so producing luminescent powders.

Differential thermal analyses (DTA) were carried out with a SETARAM TAG 16 equipment, using 30 mg of powder placed in 100 μL alumina crucibles and involving a heating rate of 10 °C min^{-1}, under synthetic air atmosphere (80% Ar + 20% O_2).

The X-ray powder diffraction (XRPD) measurements were performed at room temperature in a transmission geometry using a Bruker Advanced D8 equipment, operating at 40 kV and 45 mA, using Cu $K\alpha_1$ radiation (1.5406 Å) with a sample holder spinning at 30 rpm. The XRPD patterns were collected from 10 to 80° (2θ), with an increment of 0.013°.

2.2 Optical measurements

The luminescence spectra under continuous excitations were recorded by using three NUV-LEDs emitting at 365, 385 and 405 nm (ThorLabs model M365L2, M385L2 and M405L2, respectively). The optical power delivered on the sample was set to 1 mW. The luminescence signals were measured by a spectrometer (Avantes – AVASpec-2048 TEC), equipped with an optical fiber coupled CCD detector. The spectra were recorded with a spectral resolution of 1 nm. The internal quantum yields of powdered samples were obtained from the luminescence spectra by the Wrighton–Ginley–Morse reflection method[28] using a 50 mm integrating sphere (Avantes – AvaSphere-50). The iQY internal quantum yields were calculated following the equation: iQY = $E_s/(R_{std} - R_s)$, where E_s is the number of emitted photons from the sample, R_{std} and R_s are the number of reflected photons from the reflection standard (Spectralon) and sample, respectively. The resulting iQY values have accuracies within 5% and were determined over a series of at least four measurements for each sample. The whole setup (integrating sphere and spectrometer) was calibrated and corrected by means of a halogen 10 W tungsten lamp (Avantes – Avalight-HAL) prior the measurements.

2.3 Thermoluminescence

Thermally stimulated luminescence (TSL) measurements were carried out on samples shaped as thin pressed pellets and glued with a silver lacquer on the cold finger of a cryostat. These pellets were initially excited at 10 K across a quartz window with a UV lamp (365 nm) and TSL was detected while a heating rate of 10 K min^{-1} was applied. The detection was realized *via* an optical fiber using a Scientific Pixis 100 CCD camera (cooled at −65 °C) coupled with an Acton SpectraPro 2150i spectrometer for spectral analysis. TSL glow curves were drawn by plotting the integrated luminescence intensity over all the visible range.

2.4 Electronic paramagnetic resonance

The EPR spectra were recorded using a Bruker EMX plus equipment operating with the Bruker Xenon software. A high

sensitivity X-band resonant cavity was used and the field was controlled during the experiments with a Bruker teslameter. The spectra were recorded at 100 K, by using a Bruker nitrogen flow cryostat. DPPH was used as standard for calibration. The g-YAB powders (100 mg) were introduced inside a 4 mm diameter high purity quartz tube (Interchim Wildmad) placed into the resonant cavity.

3 Results and discussion

For the preparation of aluminoborate powders, the PP generic route was selected as this involves only environment friendly precursors. These syntheses were first based on our former works on the preparation of aluminoborate thin films for optical waveguide properties through the PP method.[29,30] In this study, the powders were first prepared involving one-step annealing, at 600–700 °C in air or under oxygen-enriched atmospheres. These direct calcinations led, in all cases, to the preparation of grey powders with very weak PL emissions. This is due to the trapping of pyrolytic carbon and to the formation of parasitic phases as carbonates coming from uncontrolled oxidations of organic precursors.[31] These unwanted impurities are detrimental to optical properties inducing significant absorption in the visible range and strong PL quenching. In order to enhance the PL properties, we developed a two-step thermal treatments to prevent any uncontrolled self-combustion process and to gradually oxidize the large amounts of organic moieties lying in the initial brown powders. These brown powders were first pyrolysed at 700 °C under nitrogen during 24 h and, in a second step, were annealed through oxygen atmosphere during 24 h at various calcination temperatures (T_{ca}). The resulting powders are shown under visible and NUV lights in Fig. 1a. The powders calcinated between 650 and 760 °C have a beige color due to absorption centers (structural defects) of these aluminoborate compounds and show intense PL emissions. On the other hand, the powders calcinated at higher temperatures (T_{ca} = 850 and 1180 °C) are white and non-luminescent under NUV excitation due to the lack of color centers, see Fig. 1a.

The structural evolutions of the aluminoborate powders as a function of calcination temperature were characterized by DTA and X-ray powder diffraction (XRPD). The DTA spectrum shown in Fig. 2 corresponds to a powder previously pyrolysed at 700 °C during 24 h and then calcinated under O_2 atmosphere at 650 °C during 24 h. These thermal treatments have allowed the release of the byproducts coming from precursor decompositions. The endothermic peak at 740 °C inducing a significant shift on the baseline is typical of a glass transition. Then, three exothermic peaks at 815, 850 and 900 °C are due to the crystallization of different phases.

On the other hand, powders prepared with different calcination temperatures, T_{ca}, were analyzed by XRPD, Fig. 3. One can observe that the powders are amorphous when calcinated at T_{ca} around the glass transition temperature, 740 °C. At T_{ca} = 780 °C, the diffraction peaks of the $Al_4B_2O_9$ (ICSD-PDF no: 76-8290) and YBO_3 (ICSD-PDF no: 89-3501) phases appear. For calcinations around 850 °C, the $YAl_3(BO_3)_4$ (c-YAB) (ICSD-PDF no: 72-1978) phase starts to crystallize, while the amount of $Al_4B_2O_9$ compound reaches a maximum and then decreases at higher temperatures. Finally, at 1180 °C we obtain the rather pure c-YAB phase with traces of YBO_3.

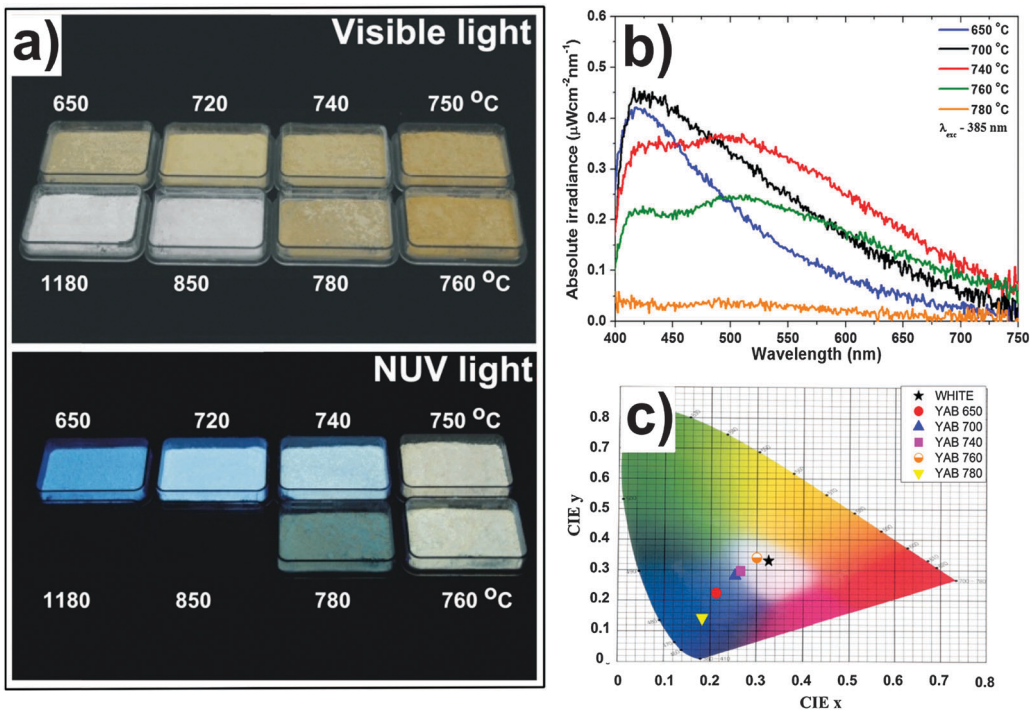

Fig. 1 (a) Aspect of powders after calcinations at different temperatures T_{ca}, observed in the visible light (up) and under near UV at 365 nm (down). (b) Evolution of PL spectra with T_{ca}, for an excitation wavelength λ_{exc} = 385 nm. (c) CIE 1931 color coordinates of the PL emission as a function of T_{ca}.

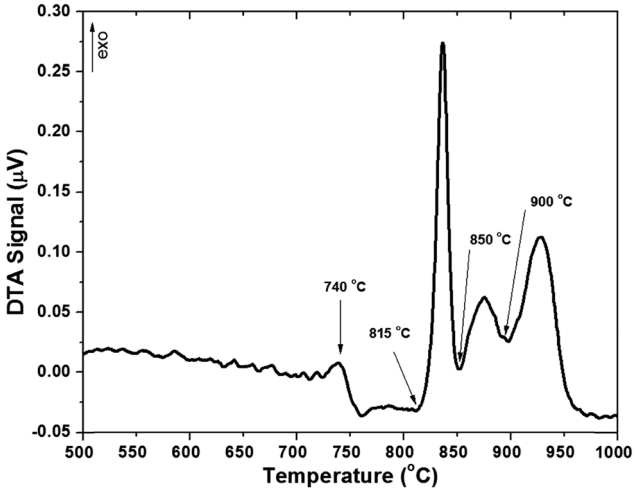

Fig. 2 DTA curve of a g-YAB powder first pyrolysed at 700 °C/24 h/N_2 and then calcinated at 650 °C during 24 h under O_2 atmosphere.

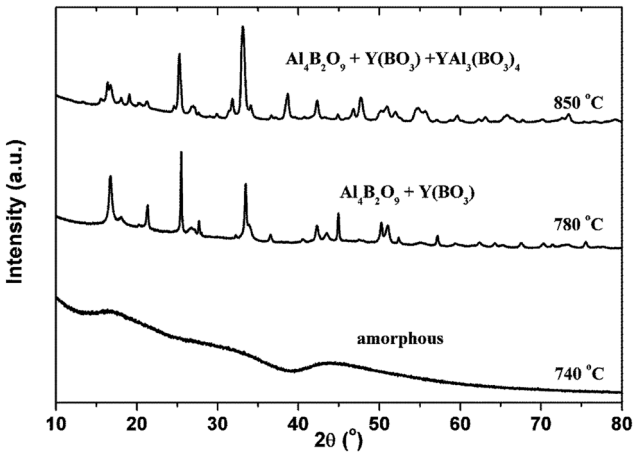

Fig. 3 XRPD of powders previously pyrolysed at 700 °C during 24 h under N_2 atmosphere and calcinated then in a second step at different temperatures T_{ca} during 24 h under O_2 atmosphere.

In conclusion to these DTA – XRPD characterizations YAB powder samples are glassy for $T_{ca} < 760$ °C with a glass transition, T_g, at around 740 °C, and exhibit the crystallization of several phases for $T_{ca} > 760$ °C. Thus, directly correlated with Fig. 1a, one can conclude that only the glassy yttrium aluminoborate (g-YAB) powders exhibit PL properties under NUV/UV excitation, and PL vanished during the crystallization due to related defect recombinations. In addition, one can notice that these PL emissions can be easily adjusted through the calcination temperature, from deep blue (T_{ca} = 650 °C) to bluish PL (T_{ca} = 700–730 °C), and finally to warmer white emissions (T_{ca} = 740–760 °C). In order to specify these promising properties, PL spectra were then recorded in the visible range.

Fig. 1b shows the PL emission spectra obtained under a 385 nm excitation wavelength, for YAB powders calcinated at different temperatures, T_{ca}. One can see that the PL spectra show broad emission bands for all $T_{ca} < 760$ °C, well extended over the whole visible region, between 400 and 750 nm. For lower T_{ca} (650 °C), the PL spectrum exhibits an intense band, centered at around 420 nm with weaker intensities above 500 nm, (blue emission, Fig. 1a). When T_{ca} is increased to 700–740 °C, the PL in the yellow-orange range increases. For 700 °C, this leads to a red-shift of the maximum of PL emission to about 515 nm. For 740 °C (glass transition temperature) the yellow-orange PL emission is further increased with the appearance of a second maximum at 515 nm, while the blue emission drops leading to an almost flat emission spectrum up to 600 nm (warmer white emission, Fig. 1a). These significant spectral evolutions with T_{ca} were confirmed by the corresponding color coordinates obtained from the PL reflection mode measurements, as seen Fig. 1c, varying from the bluish color at T_{ca} = 650 °C (CIE: x = 0.218, y = 0.225) to white color at T_{ca} = 750–760 °C (CIE: x = 0.303, y = 0.340). For $T_{ca} > 740$ °C, the PL band intensities drop very rapidly vanishing at about T_{ca} = 780–800 °C, see Fig. 1b. This PL intensity variation within a few tens of Celsius degrees of the calcination temperature is due to important structural changes occurring with the g-YAB powder crystallization. Indeed, several phases appear in that temperature range: $Al_4B_2O_9$ and (Y, Al)BO_3 compounds at around 760–770 °C, while the YBO_3, and $YAl_3(BO_3)_4$ phases start to crystallize at 780–790 °C (Fig. 3). Thus, the local reordering associated with the recrystallization of these phases have a direct impact on the point defects (color centers), which are correlated with the PL properties of the g-YAB powders.

To summarize these first results, it can be underlined that through specific annealing conditions of the g-YAB powders (temperature and atmosphere), below their crystallization temperature, it is possible to control the presence of structural defects. This allows to enhance the PL intensity and to easily tune the color emission, from blue (T_{ca} = 650–700 °C) to white (T_{ca} = 740–750 °C) that could be useful for lighting applications.[26]

A key point regarding the use of g-YAB phosphors for lighting applications, is their internal quantum yields (iQY). It has been determined as a function of T_{ca} using three excitation wavelengths λ_{exc} = 365, 385 and 405 nm (Fig. 4). For all wavelengths, iQY values increase strongly with T_{ca} from 650 to 740 °C to reach a maximum at T_{ca} = 740 °C, which corresponds to the glass transition. Moreover, internal quantum yields at these maxima are very high around 90%, 60% and 30% for excitations at 365, 385 and 405 nm, respectively. These iQY values, measured with a high reproducibility (±5%), are in good agreement with the qualitative evolutions observed on the PL emission spectra as displayed for example in Fig. 1b for λ_{exc} = 385 nm.

In complement to PL studies, thermally stimulated luminescence (TSL) gives further information of the defects depth relatively to the g-YAB phosphors energy levels. TSL spectrum presented in Fig. 5 indicates a large distribution of traps. Under excitation at 365 nm, the spectrum presents very broad components ranging from 300 K to 650 K. Since the emission as a function of temperature presented in Fig. 5 corresponds to the release of traps when the temperature is increased, the traps depths can be determine through the simple expression $E \approx 0.002T_M$,[34] where

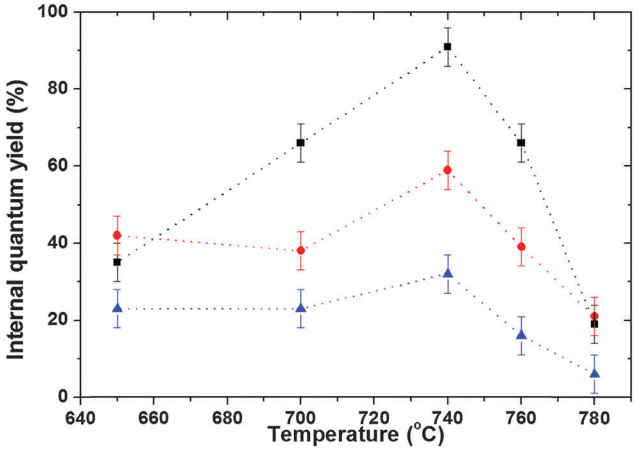

Fig. 4 Internal quantum yields as a function of calcination temperature under different excitation wavelengths, λ_{exc} = 365 nm (black squares), λ_{exc} = 385 nm (red circles) and λ_{exc} = 405 nm (blue triangles) for an optical power of 1 mW.

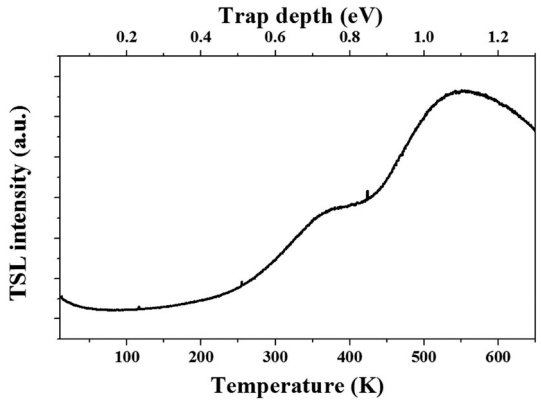

Fig. 5 Thermoluminescence spectrum registered for a g-YAB powder calcinated at T_{ca} = 740 °C.

T_M is the temperature at the peak maximum. As a very broad TSL band is observed (Fig. 5), it is quite impossible to give insights of the recombination order and process.[33] Still, one can assume that there is a rather broad distribution of the defects energy varying between ≈0.75 eV and 1.1 eV. On the other hand, the spectrum intensity is an indication of the quantity of traps.[32] The defect amount appears important, in good agreement with the high PL efficiencies observed under NUV excitation. Finally, as expected, an increase of the emission is observed with increased temperature as a higher number of traps are released. This was confirmed by others measurements presented below in this article.

To further support the idea that the origin of PL in g-YAB are also point defects as suggested for other compounds,[22] we tried to characterize these defects and how calcination influence their nature and number. We characterized the structural defects and specified their relative amounts by Electronic Paramagnetic Resonance (EPR) to then better control their formation through specific conditions of g-YAB powder annealing. These EPR measurements have been done at low temperature (100 K) on samples calcinated at different temperatures

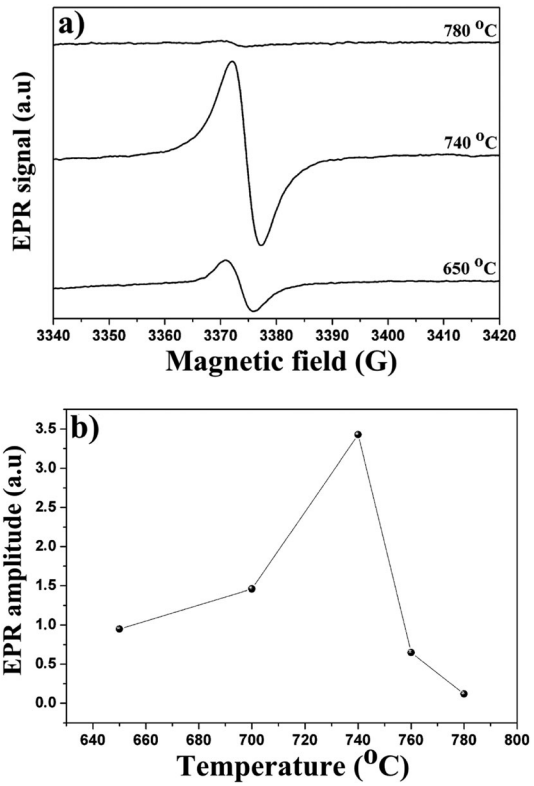

Fig. 6 (a) EPR spectra in term of the applied magnetic field. (b) EPR resonance signal amplitude (at g = 2.002) as a function of the T_{ca} calcination temperature of g-YAB powders.

(between 650 and 780 °C), Fig. 6a. The resulting EPR spectra, exhibit for all calcinated temperatures an almost isotropic signal centered at g = 2.002. It is characteristic of radical species having a spin state of S = 1/2. The intensity of this radical signal (peak-to-peak amplitude) is well correlated to the calcination temperature (Fig. 6b), hence to the PL emission. Indeed, exactly like the iQY (Fig. 4), the EPR signal increases to reach a maximum at the glass transition temperature (T_{ca} = T_g = 740 °C) and then decreases rapidly at higher temperatures with the beginning of crystallization, around 760 °C. It is noteworthy that both the EPR signal and PL intensity follow the same trend and disappear simultaneously when the powder crystallization is complete at T_{ca} > 780 °C. At the maximum of EPR resonance intensity (T_{ca} = 740 °C) the number of paramagnetic centers was estimated to be around 2.4 ± 0.4 × 10^{15} spins per gram of powder (7 ± 1 × 10^{14} spins per cm^3). Good repeatability was observed as several powder syntheses and annealings under the same conditions led to similar amounts of defects.

These directly correlated TSL, PL and EPR methods support the fact that the paramagnetic defects responsible for the EPR are the color centers at the origin of PL properties.

Regarding the precise nature of the point defect responsible for that EPR signal at g = 2.002, several hypotheses were given in the literature. Hayakawa *et al.* observed similar correlations between PL intensities and EPR signals centered at g = 2.003 in alumino-silicate glasses prepared by sol–gel chemistry.[14] EPR signals have been reported by Lin *et al.*[13] in different

amorphous luminescent hosts (Y_2O_3 and Al_2O_3) prepared by the polymeric precursors method. In both studies, the authors attributed the signal at g = 2.001–2.003 to carbon radicals (carbonyls) trapped in the host lattice during thermal treatments.[14,35] The second hypothesis suggested in the literature is oxygen-related defects, such as non-bridging oxygen (NBO) (EPR signals at g = 2.001) or peroxide radicals hole traps (PRHT,[36] O–M–O–O$^{\bullet}$, where M is a diamagnetic metal ion). In crystalline BPO_4:Ba^{2+} prepared from solutions with no carbon contamination, the PL emission (between 400 and 600 nm) was attributed to the formation of PRHT paramagnetic centers during the sample annealing (O_3–P–O–O$^{\bullet}$ and O_3–B–O–O$^{\bullet}$) associated with an EPR resonance also at g = 2.001–2.003.[19,37]

Thus, based on these previous results, one can propose that the EPR resonance recorded at g = 2.002 for the g-YAB phosphors are due to unpaired electrons hold by oxygen atoms, such as usual NBOs, or by carbon related defects such as $CO_2^{\bullet-}$ radicals. Moreover, the formation of these defects is favored around T_g temperature (740 °C) where significant structural distortions take place, leading to the maxima for EPR signals and PL intensity corresponding to the highest concentrations of paramagnetic centers (PL emitters). Then, above T_g temperature, the NBOs or carbon related defects tend to reorganize and recombine during the powder crystallization. This reduces the number of paramagnetic radicals and leads to the simultaneous decrease of EPR signals and PL intensities.

Finally, a first SSL device has been developed to estimate the lighting performances of these new phosphors. The g-YAB powders, with grain size diameters ranging between 1 and 5 μm, were dispersed in a silicone resin (Nusil LS-6257) with a mass ratio of 3 : 2. After polymerization and drying, 1.7 mm thick composite plates were cut and placed just above a NUV-LED (365 nm) in a remote phosphor configuration (Fig. 7a). The resulting basic SSL prototype (Fig. 7b) allowed the analysis of the first set of lighting characterizations in transmission mode presented Fig. 7c. The emission of the prototype showed a white emission with corresponding CIE 1931 coordinates x = 0.401, y = 0.434 and a correlated color temperature (CCT) of 4110 K. These color coordinates correspond to a warm-white lighting, comfortable for the eyes. This is indeed a very promising advantage of these g-YAB powders that was also confirmed through their PL emission spectra recorded in transmission mode (ESI,† Fig. S1). These measurements clearly indicate that the PL emission of g-YAB is constituted by a very broad PL band, spread out in the whole visible range between 430 and 750 nm, with a maximum PL intensity at around 650 nm, while that of YAG:Ce^{3+} is mainly extended in the yellow range between 500 and 670 nm with a maximum at 555 nm with CIE 1931 coordinates around x = 0.434, y = 0.552 and CCT value of 3700 K.

First characterizations have been performed to evaluate the stability of these phosphors. The PL emission of the prototype was found constant after running continuously for 24 h indicating promising photostability (Fig. S3, ESI†) but these first tests will be complemented by measurements over much longer periods (several weeks). On the other hand, the thermostability was evaluated for a g-YAB powder calcinated at T_{ca} = 740 °C. The PL spectra were recorded as a function of temperature between 25 and 300 °C (Fig. S2a, ESI†). The results clearly show that the PL intensity increases significantly (about 25%) between room temperature and 275 °C (Fig. S2b, ESI†). These results appear well reproducible, even after several heating and cooling cycles. The variation presented in Fig. S2b (ESI†) is in good agreement with the TSL measurements presented above (Fig. 5). Indeed at 275 °C (about 550 K) the release of traps is more important leading to an exaltation of TSL and PL emissions. This also clearly confirms that the emission is related to the quantity of traps in the material and in the near future, one can try to further enhance the emission by a control of the traps density. The thermostability (up to 300 °C) with even an enhanced emission at high temperature is another important advantage of the g-YAB phosphors over typical ones for high power solid-state lighting. This application requires relatively high operating temperatures (T > 120 °C) at which the YAG:Ce^{3+} phosphor displays a strikingly different behavior with an important PL intensity drop (down by 50% from room temperature to 180 °C[38,39]) in place of the increased emission reported here for g-YAB.

Based on these very promising first results, studies aiming at optimizing the elaboration of g-YAB phosphors (chemical composition, defect amount, grain size and grain morphology) are under way. On the other hand, accurate measurements of the external quantum yields of g-YAB powders and derived composites as well as optimization of the SSL prototype geometry are being performed for the development of these new phosphors and associated lighting devices.

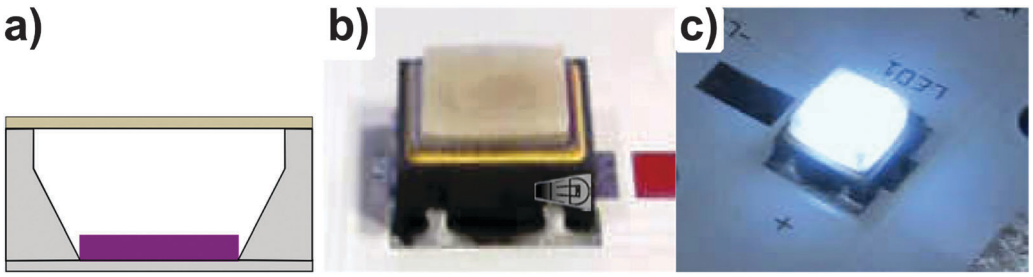

Fig. 7 (a) Schematic of the LED in remote phosphor configuration. (b) LED coupled with the composite (*ca.* 5 × 5 mm). (c) LED (365 nm) coupled with the composite under 700 mA forward bias.

4 Conclusion

We have shown that glassy yttrium aluminoborate powders, synthesized by the polymeric precursor method, exhibit intense PL broadband, extended in the whole visible range. By optimizing the thermal treatments of powders, involving a two-step process with controlled atmospheres (pyrolysis and calcination), it has been possible to gradually remove the organic moieties of precursors to avoid the formation of pyrolytic carbon or carbonate impurities, which are detrimental to PL emission (absorption and quenching). Moreover, through annealings applied near the glass transition temperature of powders, high amounts of structural defects were formed leading to high internal quantum yields under near ultraviolet excitation (iQY is around 90% at 365 nm). These iQY values constitute a record of internal PL efficiency for the defect-related phosphor family. On the other hand, one observes a direct correlation between iQY values and EPR signal amplitudes, at $g = 2.002$, suggesting that the intense white PL emission came from non-bridging oxygen or carbon impurities such as carbonyl radicals. The broadband PL emission can be explained by the presence of an important distribution of defects surrounded by a large variety of short range orders in the aluminoborate networks inducing extended energy bands within the bang-gap as confirmed by the thermally stimulated luminescence spectroscopy. Based on the promising PL efficiency of this new family of phosphors, a basic SSL prototype (WLED) has been developed to estimate the lighting performance of the g-YAB phosphors. The WLED exhibited a good thermostability associated to color coordinates (CIE 1931 $x = 0.401$, $y = 0.43$) and a correlated color temperature of 4110 K, which corresponds to a warm white emission very promising for SSL applications.

Acknowledgements

The authors acknowledge the Nanosciences Foundation of Grenoble for a PhD fellowship, the LED Engineering Development Company in Toulouse for the packaging and tests of LED devices and, on the other hand, CNRS and its CMDO network, GRAVIT-Grenoble, and finally the Brazilian agencies (CNPq, CAPES, FAPEG, FAPESP) for their financial supports.

References

1 S. T. Tan, X. W. Sun, H. V. Demir and S. P. DenBaars, *IEEE Photonics J.*, 2012, **4**, 613.
2 E. F. Schubert and J. K. Kim, *Science*, 2005, **308**, 1274.
3 S. Ye, F. Xiao, Y. X. Pan, Y. Y. Ma and Q. Y. Zhang, *Mater. Sci. Eng., R*, 2010, **71**, 1.
4 D. P. Dutta and A. K. Tyagi, *Solid State Phenon.*, 2009, **155**, 113.
5 P. Pust, V. Weiler, C. Hecht, A. Tücks, A. S. Wochnik, A. K. Henss, D. Wiechert, C. Scheu, P. J. Schmidt and W. Schnick, *Nat. Mater.*, 2014, **1**, 891.
6 W. H. Green, K. P. Le, J. Grey, T. T. Au and M. J. Sailor, *Science*, 1997, **276**, 1826.
7 V. Bekiari and P. Lianos, *Chem. Mater.*, 1998, **10**, 3777.
8 Y. Ishii, A. Matsumura, Y. Ishikawa and S. Kawasaki, *Jpn. J. Appl. Phys.*, 2011, **50**, 01AF06.
9 A. Matsumara, Y. Ishii, K. Sato, Y. Ishikawa and S. Kawasaki, *IOP Conf. Ser.: Mater. Sci. Eng.*, 2011, 102019.
10 L. S. Cavalcante, J. C. Sczancoski, J. W. M. Espinosa, V. R. Mastelaro, A. Michalowicz, P. S. Pizani, F. S. De Vicente, M. S. Li, J. A. Varela and E. Longo, *J. Alloys Compd.*, 2009, **471**, 253.
11 J. Park, J. Lee, G. R. Raju, B. K. Moon, J. H. Jeong, B. C. Choi and J. Kim, *Ceram. Int.*, 2014, **40**, 5693.
12 Y. W. W. N. Kaihatsu, F. Iskandar and K. Okuyama, *Mater. Lett.*, 2010, **64**, 836.
13 C. K. Lin, Z. Cheng, C. Zhang and Q. L. J. Meng, *Inorg. Chem.*, 2008, **47**, 49.
14 T. Hayakawa, A. Hiramitisu and M. Nogami, *Appl. Phys. Lett.*, 2003, **82**, 2975.
15 E. Orhan, M. Acinete-Santos, M. A. Maurera, F. M. Pontes, A. G. Souza, J. Andrès, A. Beltran, J. A. Varela, P. S. Pizani, A. Taft and E. Longo, *J. Solid State Chem.*, 2005, **178**, 1284.
16 M. Anicete-Santos, F. C. Picon, M. T. Escote, E. R. Leite, P. S. Pizani, J. A. Varela and E. Longo, *Appl. Phys. Lett.*, 2006, **88**, 211913.
17 F. Gu, S. F. Wang, M. K. Lu, G. J. Zhou and D. Y. D. R. Xu, *J. Phys. Chem.*, 2004, **108**, 8119.
18 Y. Hu and H.-J. Chen, *Mater. Res. Bull.*, 2008, **43**, 2153.
19 C. K. Lin, H. Luo, Z. Quan, J. Zhang, J. Fang and J. Lin, *Chem. Mater.*, 2006, **18**, 458.
20 F. Lu, X. Zhang, Z. Lu and Z. Tang, *J. Lumin.*, 2014, **149**, 231.
21 G. Dong, X. Liu, X. Xiao, Q. Zhang, G. Lin, Z. J. Ma, D. Chen and J. Qiu, *Electrochem. Solid-State Lett.*, 2009, **12**, K53.
22 C. Zhang and J. Lin, *Chem. Soc. Rev.*, 2012, **41**, 7938.
23 H. Deters, A. S. S. de Camargo, C. N. Santos, C. R. Ferrari, A. C. Hernandes, A. Ibanez, M. T. Rinke and H. Eckert, *J. Phys. Chem. C*, 2009, **113**, 16216.
24 S. Sen, Z. Xu and J. F. Stebbins, *J. Non-Cryst. Solids*, 1998, **226**, 29.
25 L. Kerns, M. C. Weinberg, S. Myers and R. Assink, *J. Non-Cryst. Solids*, 1998, **232–234**, 86.
26 A. Ibanez, V. F. Guimarães, L. J. Q. Maia and A. C. Hernandez, *European Pat.*, EP 2 468 690 A1, 2010.
27 J. K. Han, J. I. Choi, A. Piquette, M. Hannah, M. Anc, M. Galvez, J. B. Talbot and J. McKittricka, *ECS J. Solid State Sci. Technol.*, 2013, **2**, R3138.
28 M. S. Wrighton, D. S. Ginley and D. L. Morse, *J. Phys. Chem.*, 1974, **78**, 2229.
29 L. J. Q. Maia, C. R. Ferrari, V. R. Mastelaro, A. C. Hernandes and A. Ibanez, *Solid State Sci.*, 2008, **10**, 1835.
30 L. J. Q. Maia, A. Ibanez, L. Ortega, V. R. Mastelaro and A. C. Hernandes, *J. Nanopart. Res.*, 2008, **10**, 1251.

31 J. F. Carvalho, F. S. de Vicente, S. Pairis, P. Odier, A. C. Hernandes and A. Ibanez, *J. Eur. Ceram. Soc.*, 2009, **29**, 2511.
32 A. Lecointre, A. Bessière, A. J. J. Bos, P. Dorenbos, B. Viana and S. Jacquart, *J. Phys. Chem. C*, 2011, **115**, 4217.
33 J. Randall and M. Wilkins, *Proc. R. Soc. London, Ser. A*, 1945, **184**, 366.
34 A. J. J. Bos, *Radiat. Meas.*, 2006, **41**, S45.
35 C. Lin, C. Zhang and J. Lin, *J. Lumin.*, 2009, **129**, 1469.
36 H. Sun, S. Juodkazis, M. Watanabe, S. Matsuo and H. Misawa, *J. Phys. Chem. B*, 2000, **104**, 3450.
37 J. Huang, H. Luo, X. Yu, Y. Li and W. Zou, *J. Lumin.*, 2008, **128**, 589.
38 H. Shi, C. Zhu, J. Huang, J. Chen, D. Chen, W. Wang, F. Wang, Y. Cao and X. Yuan, *Opt. Mater. Express*, 2014, **4**, 649.
39 Q. Shao, Y. Dong, J. Jiang, C. Liang and J. He, *J. Lumin.*, 2011, **131**, 1013.